ACS Catalysis

Research Article

pubs.acs.org/acscatalysis

Selective Hydrogenation of Phenol Catalyzed by Palladium on High-Surface-Area Ceria at Room Temperature and Ambient Pressure

Nicholas C. Nelson,[†,‡] J. Sebastián Manzano,[†,‡] Aaron D. Sadow,[†,‡] Steven H. Overbury,[§] and Igor I. Slowing*[,†,‡]

[†]US DOE Ames Laboratory, Ames, Iowa 50011, United States

[‡]Department of Chemistry, Iowa State University, 1605 Gilman Hall, Ames, Iowa 50011, United States

[§]Oak Ridge National Laboratory, P.O. Box 2008, Oak Ridge, Tennessee 37831, United States

Supporting Information

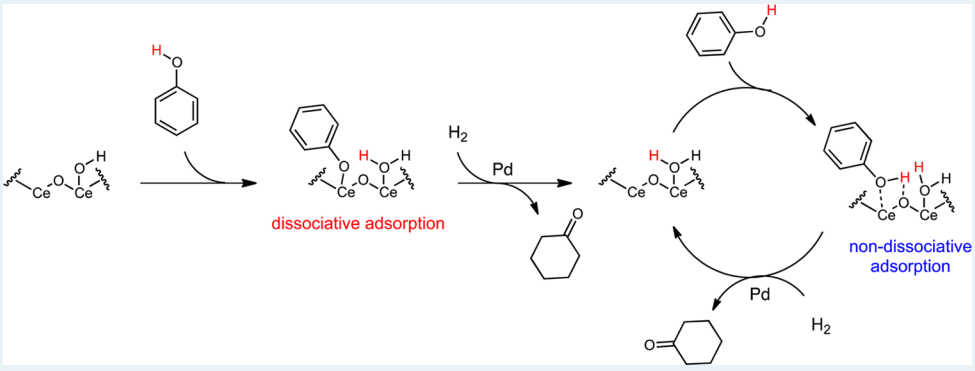

ABSTRACT: Palladium supported on high-surface-area ceria effectively catalyzes the hydrogenation of phenol to cyclohexanone at atmospheric pressure and room temperature. Activation of H_2 at Pd sites and phenol at surface ceria sites was investigated by probing the redox properties of the catalyst and studying the mechanism of phenol adsorption. Temperature-programmed reduction and pulsed chemisorption were used to examine the effects of prereduction temperature on catalyst dispersion and reducibility. A sharp effect of prereduction temperature on catalytic activity was observed. This dependence is rationalized as a result of interactions between palladium and ceria, which under reducing conditions enhance palladium dispersion and create different types of environments around the Pd active sites and of encapsulation of the catalyst caused by support sintering at high temperatures. Temperature-programmed diffuse reflectance infrared Fourier transform spectroscopy revealed that phenol undergoes dissociative adsorption on ceria to yield cerium-bound phenoxy and water. Reduction of the chemisorbed phenoxy species decreases the number of proton-accepting sites on the surface of ceria and prevents further dissociative adsorption. Subsequent phenol binding proceeds through physisorption, which is a less active binding mode for reduction by hydrogen. High activity can be restored upon regeneration of proton acceptor sites via reoxidation/reduction of the catalyst.

KEYWORDS: *mesoporous ceria, phenol hydrogenation, metal−support interactions, dissociative adsorption, redox-active support*

INTRODUCTION

Cyclohexanone is a precursor to caprolactam and adipic acid, which are key intermediates for the synthesis of nylons and polyamide resins. Cyclohexanone is commercially produced by oxidation of cyclohexane or hydrogenation of phenol.[1] The former route involves high reaction temperatures (140−180 °C) and pressures (8−20 bar) and low conversion (<10%).[1,2] Phenol hydrogenation is much more efficient and is catalyzed by palladium on carbon (Pd/C) in the liquid phase and by palladium on alumina (Pd/Al_2O_3) in the vapor phase.[3] Of the two hydrogenation approaches, liquid-phase reduction is more selective to the ketone but operates at high temperatures (175 °C) and under excess hydrogen pressures (13 bar).[1,3] Given the importance of this process, significant efforts have been devoted to the development of alternative catalysts that can further improve yields and enable conversion under milder conditions. Several research groups have now achieved remarkable results with conversion and selectivity over 90% at either room temperature or 1 bar of H_2 pressure.[4−16] The most efficient processes take advantage of the fact that aromatics can be reduced under mild conditions when the activation of H_2 by heterogeneous Pd catalyst is combined with the electrophilic activation of aromatics by soluble Lewis acids.[17] Liu et al. demonstrated the application of this strategy for the hydrogenation of phenol by combining Pd/Al_2O_3 with $AlCl_3$.[7] Lee and co-workers significantly improved the process by

Received: December 12, 2014
Revised: February 5, 2015
Published: February 18, 2015

DOI: 10.1021/cs502000j
ACS Catal. 2015, 5, 2051−2061

combining $Sc(OTf)_3$ with Pd/C, achieving full conversion at 20 °C and 1 bar of H_2.[8] The Lewis acid also favors the selectivity to the cyclohexanone by forming an adduct that is more difficult to reduce to the alcohol. Li, Luque, and collaborators achieved similar results with a fully heterogeneous system using Pd supported on the chromium-based MOF MIL-101, with the chromium centers in the MOF support proposed as Lewis acidic activators for the reaction.[11]

The strategy of using the support as an active component of the reaction rather than as an inert, inactive component merely for catalyst dispersion is particularly attractive from the perspective of advanced catalyst design. In this regard, redox-active supports are especially appealing, as they have the potential of participating in electron transfer processes during catalysis. Cerium dioxide (ceria) is an interesting support for this purpose because of its reducibility and its interactions with noble metals.[18] These interactions lead to high dispersion of catalytic metals and provide beneficial electronic effects.[19] Ceria and ceria-based materials have been extensively studied as structural and electronic promoters to improve the activity and selectivity of heterogeneous catalysts.[20] Ceria is the most industrially significant rare earth oxide catalyst mainly due to its use in three-way catalytic converters (TWC) and fluid catalytic cracking (FCC).[19,21] Recently, ceria-based materials have been investigated for use in soot removal from diesel engine exhausts,[22] volatile organic compound (VOC) degradation,[23] fuel cell technology,[24] water-gas shift reaction,[25,26] preferential CO oxidation (PROX),[27] oxidative dehydrogenation,[28] and selective hydrocarbon oxidations.[29,30] The success of ceria and ceria-based materials in catalysis is oftentimes due to facile Ce^{4+}/Ce^{3+} redox cycling without disruption of the fluorite lattice structure.[20] Furthermore, the redox properties of ceria-based materials can be tuned by incorporation of dopants or deposition of metals, which offer significant opportunities for modifying their activity and improving their performance.[31]

Only a few studies exist for phenol hydrogenation on ceria-based materials. The groups of Inagaki and Scire studied the reaction in the vapor phase over palladium supported on high-surface-area ceria (Pd/CeO_2) at 180 °C (80% conversion, 50% selectivity) and 160 °C (40% conversion, 95% selectivity), respectively.[32,33] The liquid-phase process was investigated by Li et al. using Ce-doped Pd nanospheres (0.43 mol % Ce) with a hollow chamber, obtaining an 82% cyclohexanone yield under 10 bar of H_2 at 80 °C.[34] In another paper, Li and co-workers used palladium−cerium−boron supported on hydrotalcite to achieve 82% conversion and 80% selectivity within 4 h at 10 bar of H_2 and 100 °C.[35] Using ceria as the support rather than as a minor component of the catalyst may be a good way to take advantage of its redox properties and its electronic effects on the metal in the liquid-phase process. Furthermore, using high-surface-area ceria as a support should result in higher activity in comparison to a low-surface-area counterpart, because this could lead to increased dispersion of the supported metal and larger amounts of reactive species on the surface.[36] Herein, we report the synthesis of palladium supported on high-surface-ceria (Pd/CeO_2) and its exceptional performance for the selective hydrogenation of phenol to cyclohexanone in the liquid phase at low temperature and H_2 pressure.

EXPERIMENTAL SECTION

Reagents. Cerium(III) nitrate hexahydrate ($Ce(NO_3)_3{\cdot}6H_2O$), palladium(II) acetate ($Pd(O_2CCH_3)_2$), phenol (C_6H_5OH), tetramethylorthosilicate (TMOS), aluminum(III) isopropoxide ($Al(OiPr)_3$), cerium(IV) oxide (CeO_2), 10 wt % palladium supported on carbon (Pd/C), and concentrated nitric acid were purchased from Sigma-Aldrich. Pluronic P104 and Pluronic P123 were obtained from BASF. $Ce(NO_3)_3{\cdot}6H_2O$ was dried under vacuum at room temperature prior to synthesis. Ethyl alcohol (100%) was used for all syntheses. All other chemicals were used without further purification.

Synthesis of High-Surface-Area Ceria (CeO_2). In a typical synthesis, $Ce(NO_3)_3{\cdot}6H_2O$ (8.80 g, 20.3 mmol) and the nonionic block copolymer surfactant Pluronic P104 (10.1 g, 1.71 mmol) were dissolved in ethanol (200 mL) with vigorous stirring (700 rpm) for 3 h. Once thoroughly homogenized, the solution was cast into a large crystallization dish (diameter 185 mm) and placed into a preheated 65 °C oven to undergo solvent evaporation. After 12−24 h, the gel was placed into a preheated 150 °C oven for an additional 12 h. To remove the remaining P104 surfactant, the yellow powder was calcined in air at 450 °C for 4 h with a ramp rate of 1 °C min^{-1}. Optimal surface areas were obtained when the relative humidity was kept below 60%. *Caution!* During thermal treatment at 150 °C, combustion occurs within ∼12 min, producing flames which self-extinguish within seconds after all combustible material (i.e., block copolymer) is burned. The thermal treatment step should be conducted in an oven, preferably in a fume hood to avoid exposure to gaseous decomposition products.

Synthesis of Mesoporous Silica (SiO_2). This material was prepared by following our previously published method.[37] Pluronic P104 (7.00 g, 1.19 mmol) was dissolved in aqueous HCl (273.0 g, 1.6 M). After the solution was stirred for 1 h at 56 °C, tetramethylorthosilicate (10.6 g, 69.9 mmol) was added and the mixture was stirred (500 rpm) for an additional 24 h. The resulting mixture was hydrothermally treated for 24 h at 150 °C in a high-pressure reactor. Upon cooling to room temperature, the white solid was collected by filtration, washed with copious amounts of methanol, and dried in air. The MSN material was calcined in air at 550 °C for 6 h with a ramp rate of 1.5 °C min^{-1}.

Synthesis of Mesoporous Alumina (Al_2O_3). The synthesis of alumina was adapted from the method of Yan and co-workers.[38] Briefly, nonionic block copolymer surfactant Pluronic P123 (0.92 g, 0.16 mmol) was dissolved in ethanol (20 mL) at room temperature. After the solution was stirred for 0.5 h, concentrated nitric acid (1.5 mL, 15.8 M) and $Al(OiPr)_3$ (2.04 g, 10.0 mmol) were added with vigorous stirring (800 rpm). The mixture was capped, stirred at room temperature for 5 h, and then cast into a large crystallization dish. The dish was placed into a preheated 60 °C oven to undergo solvent evaporation for 48 h. The light yellow solid was calcined in air at 400 °C for 6 h with a ramp rate of 1.5 °C min^{-1}.

Synthesis of Pd/M_xO_y. All Pd catalysts were prepared by an impregnation method with a 1 wt % Pd loading relative to the mass of the support. In a typical synthesis, $Pd(O_2CCH_3)_2$ (0.0419 g, 0.187 mmol) was dissolved in acetone (1 mL). The support (2.00 g) was placed in a mortar and impregnated with the Pd solution in 0.20 mL increments. After each impregnation step, the catalyst was mixed thoroughly with a pestle until seemingly dry. The material was calcined at 350 °C for 2 h with a 2.5 °C min^{-1} ramp rate and then reduced under flowing hydrogen at 350 °C for 2 h with a ramp rate of 2.5 °C min^{-1}. *Caution!* Special precautions should be taken when preparing (i.e., reducing) Pd/Al_2O_3, as pyrophoric aluminum hydrides may form. The physicochemical properties of non-ceria-based catalysts are reported in Table S1 in the Supporting Information.

Hydrogenation Reactions. All reactions were conducted in batch mode under flowing hydrogen (∼1 bar) using a Schlenk line. In a typical experiment, the catalyst (48 mg, 1.1 wt % Pd loading) and phenol solution (4 mL, 0.025 M) were added to a 10 mL round-bottom flask equipped with a condenser and stir bar. The palladium to substrate ratio was maintained at 5 mol % for all reactions. The flask was placed on a Schlenk line under a headspace flow of hydrogen, and the contents were stirred (800 rpm) for 4 h. The reaction product was collected by centrifugation. A 50 μL aliquot of the supernatant was added to 1 mL of ethanol and analyzed in an Agilent GC-MS instrument (7890A, 5975C) with a HP-5MS column. The run started at 60 °C, and the temperature was then ramped to 150 °C at 5 °C

DOI: 10.1021/cs502000j
ACS Catal. 2015, 5, 2051−2061

min^{-1}. Then the temperature was ramped to 300 °C at 20 °C $min^{-1}$and then it was held at 300 °C for 3 min. Resorcinol was used as an internal standard. Conversion was defined as mole percent and calculated as moles of converted phenol per mole of starting phenol times 100%. The selectivity was defined as mole percent and calculated as moles of cyclohexanone per moles of products times 100%. Yields were defined as mole percent and were calculated as moles of each product multiplied by conversion times 100%.

TPR and Chemisorption. Hydrogen temperature-programmed reduction (H_2-TPR) and hydrogen chemisorption were performed in a Micromeritics AutoChem II instrument. H_2 in Ar (H_2/Ar) (10.13%) was used as the reducing agent or metal dispersion probe. H_2-TPR experiments were performed with a flow rate of 50 mL min^{-1} and a ramp rate of 10 °C min^{-1}. A cold trap was used to collect water produced during the reduction. H_2-chemisorption analysis was carried out by reducing samples at specified temperatures and then heating/cooling to 250 °C under H_2/Ar, followed by flowing Ar for 15 min at 250 °C to remove surface-bound hydrogen from Pd crystallites. The sample was then cooled under Ar to −35 °C for hydrogen pulse chemisorption measurements. The palladium dispersion of the catalysts was calculated on the basis of the equation

$$D\ (\%) = \frac{S_f M V_{ad}}{m W V_m} \times 100$$

where S_f = stoichiometry factor (Pd/H_2 molar ratio) = 2, M = atomic mass of Pd (106.42 g mol^{-1}), V_{ad} = volume of chemisorbed H_2 (mL) under standard temperature and pressure (STP) conditions, m = mass of the sample (g), W = weight fraction of Pd in the sample as determined by ICP-OES (0.011 g of Pd/g of sample), and V_m = molar volume of H_2 (22414 mL mol^{-1}) under STP conditions.

The specific surface area of palladium was calculated on the basis of the equation

$$\text{Pd surface area } (m^2\ g^{-1} \text{ of Pd}) = \frac{S_f N_A SA_{cross} V_{ad}}{m W V_m}$$

where S_f = stoichiometry factor (Pd/H_2 molar ratio) = 2, N_A = Avogadro's number (6.023×10^{23} mol^{-1}), SA_{cross} = palladium cross-sectional area (7.87×10^{-20} m^2), V_{ad} = volume of chemisorbed H_2 under STP conditions (mL), m = mass of the sample (g), W = weight fraction of Pd in the sample as determined by ICP-OES (0.011 g of Pd/g of sample), and V_m = molar volume of H_2 (22414 mL mol^{-1}) under STP conditions.

The cubic crystallite size of palladium was calculated on the basis of the equation

$$\text{Pd crystallite size (nm)} = \frac{6M}{m W d_{Pd} N_A SA_{Pd}}$$

where M = atomic mass of Pd (106.42 g mol^{-1}), m = mass of the sample (g), W = weight fraction of Pd in the sample as determined by ICP-OES (0.011 g of Pd/g of sample); d_{Pd} = density of palladium (1.202×10^{-20} g nm^{-3}), N_A = Avogadro's number (6.023×10^{23} mol^{-1}); SA_{Pd} = palladium surface area from the equation above (nm^2/g of Pd). The number 6 is derived from assuming cubic geometry.

Powder X-ray Diffraction (PXRD). Diffraction patterns were collected using Co Kα1, Kα2 split radiation (45 kV, 40 mA, λ_{avg} = 1.7903 Å) on a PANalytical X'Pert PRO diffractometer equipped with a θ–θ vertical mode goniometer, incident Fe filter, an air-cooled X'Celerator real time multiple strip (RTMS) detector, and a spinner stage. The spectra were converted to Cu Kα radiation for comparison to standard patterns. Powder XRD samples were prepared by placing powders onto a background-less polycarbonate sample holder. Crystallite sizes were calculated using the Scherrer equation:

$$D_{hkl} = \frac{K\lambda}{\beta \cos\theta}$$

where K is the shape factor (0.9) of the average crystallite, λ is the X-ray wavelength (0.17903 nm), β is the full width at half-maximum (radians), and θ is the Bragg angle (radians).

Electron Microscopy/Energy Dispersive X-ray Spectroscopy. Transmission electron microscopy (TEM) was conducted using a FEI Technai G2 F20 field emission microscope and scanning transmission electron microscope (STEM) operating at 200 kV (point-to-point resolution <0.25 nm and a line-to-line resolution of <0.10 nm). TEM samples were prepared by placing 2–3 drops of dilute ethanol suspensions onto lacey-carbon-coated copper grids. The compositions of Pd/CeO_2 structures were characterized by elemental mapping and energy dispersive X-ray spectroscopy (EDS) scans in STEM mode.

Surface Area and Porosimetry. Textural properties of the supports and catalysts were measured by nitrogen sorption isotherms at −196 °C in a Micromeritics Tristar analyzer. The surface areas were calculated by the Brunauer–Emmett–Teller (BET) method, and the pore size distribution was calculated by the Barrett–Joyner–Halenda (BJH) method. Pretreatment of samples for surface area measurement was done under flowing N_2 for 6 h at 100 °C.

ICP-OES. Pd loadings were analyzed in a PerkinElmer Optima 2100 DV inductively coupled plasma–optical emission spectroscope (ICP-OES). Samples (5 mg) were digested for 24 h in aqueous HF and HCl solution (0.18 and 5 v/v %, respectively).

Diffuse Reflectance Infrared Fourier Transform (DRIFT). Measurements were made on a Bruker Vertex 80 FT-IR spectrometer with OPUS software and apodized spectral resolution of 0.2 cm^{-1}. The spectrometer was equipped with a HeNe laser and photovoltaic MCT detector. A Praying Mantis diffuse reflectance accessory and high-temperature reaction chamber were used for room-temperature and variable-temperature measurements, respectively.

Diffuse Reflectance UV/Visible Absorption Spectroscopy (DR UV/vis). Measurements were made on an Ocean Optics USB2000+ fiber optic spectrometer (bandwidth 350–1100 nm) operating in absorption mode. Samples were prepared by suspending 50 mg of ceria in 0.5 mL of phenol dissolved in test solvents (33 mg mL^{-1}) overnight. The solid was collected by centrifugation and analyzed.

Nuclear Magnetic Resonance. Proton nuclear magnetic resonance (^{1}H NMR) spectra were collected on a Varian VXR-300 equipped with a narrow bore 7.05 T/300 MHz magnet and a standard ^{1}H probe. Deuterated benzene and cyclohexane were used as solvent and internal standard, respectively.

X-ray Photoelectron Spectroscopy (XPS). XPS analysis was done with a PHI 5500 multitechnique system using a standard Al X-ray source. The Pd/CeO_2 catalyst exposed to air was prepared by deposition onto a double-sided-tape sample holder. The Pd/CeO_2 catalyst exposed to hydrogen was prepared in a glovebox and then transferred to the XPS chamber in an air-free sample cell. Charge correction was accomplished by shifting the O 1s peak to 529.0 eV for all spectra.[39]

RESULTS AND DISCUSSION

Support Synthesis and Characterization. The ceria support was synthesized by an evaporation-induced self-assembly method (EISA) commonly used for the synthesis of high-surface-area metal oxides.[40−43] The physical properties of the CeO_2 support and Pd/CeO_2 catalyst are summarized in Table 1. The PXRD pattern measured was indexed to the fluorite cubic structure of ceria (space group *Fm3m* (No. 225),

Table 1. Physical Properties of CeO_2 Support and Pd/CeO_2 Catalyst

sample	BET surface area ($m^2\ g^{-1}$)	BJH pore volume ($cm^3\ g^{-1}$)	CeO_2 crystallite size (nm)[a]	Pd dispersion (%)[b]	Pd crystallite size (nm)[b]
CeO_2	241	0.31	5.9		
Pd/CeO_2	159	0.27	7.1	64	1.5

[a]Obtained by PXRD analysis. [b]Obtained by H_2 chemisorption.

DOI: 10.1021/cs502000j
ACS Catal. 2015, 5, 2051−2061

JCPDS 34-0394) (Figure 1a). The broad peaks indicated small ceria crystallites, and estimation of the average crystallite size

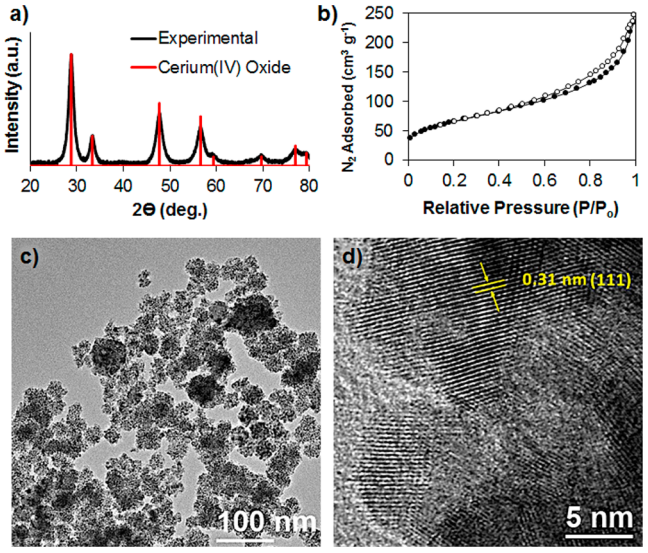

Figure 1. (a) Wide-angle PXRD pattern of the synthesized CeO_2 (black) and reference cerium(IV) oxide (red). (b) N_2 sorption isotherms of CeO_2. (c) TEM and (d) HR-TEM images of CeO_2 showing a *d* spacing of 0.31 nm corresponding to the (111) planes of CeO_2.

using the Scherrer equation provided a value of 5.9 nm. Nitrogen sorption analysis gave a high specific surface area and displayed a hysteresis loop at high partial pressures, suggesting significant textural porosity (Figure 1b). TEM imaging revealed that the material is comprised of aggregated particles with small voids within each aggregate that likely account for the measured pore volume (Figure 1c). HR-TEM (Figure 1d) examination indicated the presence of the most thermodynamically stable (111) planes of the cubic lattice.[31] Given the polycrystalline nature of the material, (200) and (220) planes were also observed, although they were far less prevalent than the (111) planes.

Catalyst Synthesis and Characterization. The catalyst was prepared via incipient wetness impregnation. An acetone solution of palladium(II) acetate was initially added to the ceria material; the mixture was then calcined in air to produce the PdO_xH_y/CeO_2 precatalyst, which was finally reduced by flowing hydrogen at 350 °C to give the Pd/CeO_2 catalyst. The PXRD pattern of Pd/CeO_2 is nearly identical with that of CeO_2 (Figure 2a). The ceria reflections of the catalyst are slightly narrower than those of the original support, suggesting that sintering occurred during the additional thermal aging, which is common for ceria in reducing environments.[44] This sintering likely led to the lowered specific surface area and pore volume of Pd/CeO_2 relative to that of CeO_2 (Table 1). Palladium species could not be detected by XRD analysis, suggesting it was highly dispersed over the support[45] and/or incorporated into the ceria framework.[46] The rationalization of highly dispersed palladium is consistent with the low loading of palladium (1.1 wt % as determined by ICP-OES) and its high affinity for ceria.[47] In support of this idea, sub-ambient-pressure H_2 chemisorption measurements gave a high Pd dispersion of 64% and a calculated cubic crystallite size of 1.5 nm. The catalyst was further investigated by STEM-HAADF imaging (Figure 2b). Palladium particles could not be directly observed,

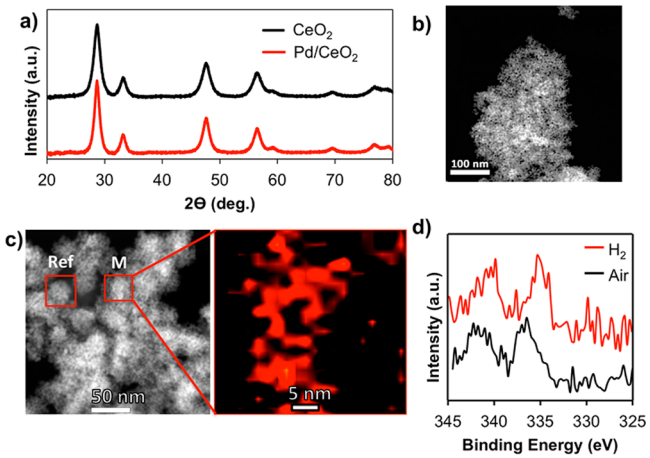

Figure 2. (a) Wide-angle PXRD patterns of CeO_2 support (black) and Pd/CeO_2 catalyst (red). (b) STEM-HAADF image of Pd/CeO_2. (c) EDS map of Pd (red image) on a 25 × 25 square section of the support (region M). The square labeled "Ref" was taken as a reference for drift correction between scans. (d) X-ray photoelectron spectra of Pd/CeO_2 exposed to air (black) and to hydrogen atmosphere (red).

possibly due to high dispersion, small crystallite size, and/or low contrast between Pd and Ce. However, energy dispersive X-ray spectroscopy (EDS) mapping confirmed the presence of Pd on the support (Figure 2c and Figure S2 in the Supporting Information). XPS analysis was also used to evaluate the oxidation state of palladium in the catalyst. The binding energy of Pd $3d_{5/2}$ electrons in the catalyst exposed to ambient air (336.5 eV) is close to that in PdO (336.9 eV), suggesting that part of the metal, likely the atoms at the surface, is easily oxidized in air (Figure 2d, black trace).[39] Exposure of the catalyst to H_2 at room temperature (a more accurate description of the catalyst under catalytic conditions) shifts the binding energy to lower values (335.2 eV), suggesting significant conversion to the metallic form (Figure 2d, red trace).

H_2-TPR experiments were run on CeO_2 and the precatalyst (PdO_xH_y/CeO_2) to study the effect of Pd impregnation on the redox properties of the material (Figure 3). The results are

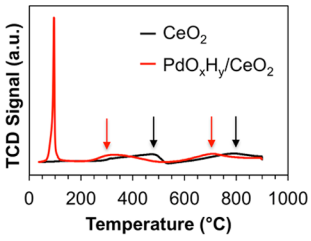

Figure 3. H_2-TPR profiles of CeO_2 (black) and PdO_xH_y/CeO_2 (red).

summarized in Table 2. Upon hydrogen treatment of CeO_2, two peaks were observed corresponding to reduction of surface

Table 2. Reducibility of CeO_2 Support and PdO_xH_y/CeO_2 Precatalyst

	H_2 consumed (mmol g^{-1})			
sample	at T_1	at T_2	at T_3	total
CeO_2		0.69	1.1	1.79
PdO_xH_y/CeO_2	0.98	0.63	0.58	2.19

DOI: 10.1021/cs502000j
ACS Catal. 2015, 5, 2051−2061

and bulk ceria at 473 °C (T_2) and 791 °C (T_3), respectively.[48] Overall, the amount of H_2 consumed in the pure CeO_2 sample was less than the total amount consumed by the PdO_xH_y/CeO_2 precatalyst. There was considerable hydrogen consumption by the PdO_xH_y/CeO_2 precatalyst at 95 °C (T_1), which can be attributed, in part, to the reduction of PdO_xH_y species.[49] Interestingly, the PdO_xH_y/CeO_2 precatalyst consumed less H_2 at the higher temperatures associated with surface and bulk ceria reduction than the Pd-free CeO_2 support. Thus, the presence of Pd facilitated the reduction of surface and bulk CeO_2, as indicated by the lower reduction temperatures in comparison to the support alone (332 °C for T_2 and 703 °C for T_3). The total amount of hydrogen consumed by PdO_xH_y/CeO_2 was 0.40 mmol H_2 g^{-1} greater than the amount consumed by the CeO_2 support (Table 2). Assuming that Pd is in the +2 oxidation state, this is 4 times greater than the theoretical amount of hydrogen that ought to be consumed (0.10 mmol H_2 g^{-1}) to reduce PdO to Pd on the basis of ICP results. If all Pd atoms formed hydrides, this would imply consumption of an additional 0.05 mmol H_2 g^{-1}, which would still leave 0.25 mmol H_2 g^{-1}. This difference suggests hydrogen spilled over onto the support during the reduction of PdO_xH_y, which could have either been physisorbed or led to the reduction of ceria.[50] A significant decrease in the amount of hydrogen consumed by the PdO_xH_y/CeO_2 catalyst at high temperatures (Table 2) relative to that of the CeO_2 support suggested that some hydrogen spilled over, leading to the reduction of ceria. These results are consistent with previous hydrogen adsorption studies for palladium on ceria catalysts.[50] Hydrogen spillover is common in reducible oxides serving as supports for noble metals.[51]

The TPR profile of the PdO_xH_y/CeO_2 precatalyst (Figure 3) suggested that complete reduction of Pd is achieved at temperatures above 125 °C. The effects of PdO_xH_y/CeO_2 reduction temperature on the redox properties of the catalyst were further evaluated on the basis of literature reports of the significant structural changes observed for noble metals supported on ceria under reducing conditions.[47] To this end, four Pd/CeO_2 samples were produced by reduction of PdO_xH_y/CeO_2 precatalyst at 150, 250, 350, and 450 °C, respectively. Each sample was then reoxidized (350 °C under an O_2/He mixture for 1 h, 10 °C min^{-1}) to examine their reducibility as a function of pretreatment temperature. The TPR analysis revealed significant effects of the prereduction temperature on the H_2 uptake of the catalyst (Figure 4). PdO_xH_y/CeO_2 prereduced at 150 °C consumed hydrogen near room temperature (28 °C), but there was also considerable hydrogen uptake at the same temperature as that for the original precatalyst (95 °C). Pretreatment of PdO_xH_y/CeO_2 under H_2 at 250 or 350 °C resulted in only one peak centered at 28 and 14 °C, respectively. PdO_xH_y/CeO_2 prereduced at 450 °C showed three hydrogen consumption peaks at 8, 25, and 51 °C. These changes could be due to interactions between Pd and CeO_2 and structural transformations undergone by CeO_2 as the reduction temperature increases, which have been well documented for noble metals supported on ceria under reducing conditions.[47] Thus, increasing reduction temperatures may lead to incremental spreading of Pd over CeO_2 to give smaller particles that are reactive at lower temperatures, as indicated by the shift in the TPR peak from 95 °C to 28 °C and 14 °C. While reduction of the precatalyst at 450 °C led to further shifting of the signal to 8 °C, additional peaks appeared at 25 and 51 °C. These higher temperature H_2 uptake peaks

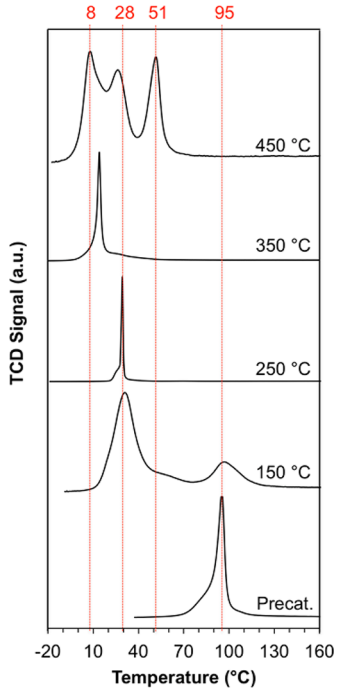

Figure 4. H_2-TPR profiles of PdO_xH_y/CeO_2 precatalyst reduced at 150, 250, 350, and 450 °C. To measure the TPR, each sample was previously reoxidized at 350 °C. TPR of the precatalyst is included at the bottom as a reference. Temperatures of selected peaks are indicated in red at the top of the figure.

can be attributed to the metal existing in different types of environments that involve additional interactions with CeO_2, such as decoration phenomena (i.e., burial of surface palladium by sintered ceria),[47,52] alloying of Pd−Ce,[53] and/or electronic support effects.[31]

Dispersion measurements were taken on the catalysts after the initial reduction in order to further evaluate the changes in Pd surface with reduction temperature (Figure S1 in the Supporting Information). Measurements were performed at −35 °C to eliminate erroneous results from hydrogen spillover.[31,54] The results revealed that, indeed, Pd dispersion increased as the reduction temperature increased from 150 to 350 °C. Sanchez and Gazquez[52] proposed a model to explain the changes in dispersion of metals in oxide supports upon reduction at high temperatures. In their model, they proposed the occupancy of oxygen ion vacancies by metal atoms; as the reduction temperature increases, more vacancies are formed, which lead to migration of Pd crystallites into these high-energy environments, resulting in increased dispersion. Part of the hydrogen consumed by PdO_xH_y/CeO_2 prereduced at 150 °C was observed at the same temperature (95 °C) as that of the original precatalyst (Figure 4). This suggests that some Pd crystallites remained in the same environment as they were upon deposition of the $Pd(O_2CCH_3)_2$ precursor and calcination in air, while others relocated to a different environment. As the prereduction temperature was increased to 250 °C, only one peak (28 °C) was observed, which coincided with part of the hydrogen uptake temperature for the catalyst prereduced at 150 °C (Figure 4). These data are consistent with the Pd species spreading over different sites on the surface of CeO_2. Recent studies have shown that surface oxygen vacancies promote late-transition-metal dispersion over ceria supports.[55,56] Prereduction at 350 °C resulted in one peak

DOI: 10.1021/cs502000j
ACS Catal. 2015, 5, 2051−2061

Table 3. Reaction Conditions and Results for the Hydrogenation of Phenol in Hexane

					selectivity (%)	
entry	catalyst	T (°C)	t (h)	conversion (%)	C=O	OH
1	CeO_2	25	4	0.0		
2	PdO_xH_y/CeO_2	25	4	0.0		
3	Pd/CeO_2	25	4	86.2 ± 1.8[c]	96.3 ± 1.4	3.7 ± 1.4
4	Pd/CeO_2	35	4	94.1 ± 0.4	90.8 ± 3.4	9.2 ± 3.4
5	Pd/Al_2O_3	25	4	7.4 ± 3.4	100.0 ± 0.0	0.0
6	Pd/SiO_2	25	4	36.6 ± 3.3	100.0 ± 0.0	0.0
7[a]	Pd/C	25	4	42.7 ± 2.5	95.4 ± 2.6	4.6 ± 2.6
8[b]	Pd/CeO_2	25	4	62.5 ± 3.6	96.2 ± 2.0	3.8 ± 2.0

[a]Commercial Pd/C. [b]Commercial ceria. [c]Standard deviations calculated from three different catalytic runs.

at 14 °C (Figure 4). Interestingly, this prereduction temperature corresponded to the temperature for reduction of surface ceria (i.e., vacancy formation) in the PdO_xH_y/CeO_2 precatalyst (Figure 3 (red)). Prereduction of PdO_xH_y/CeO_2 at 450 °C led to a dramatically lower dispersion in comparison to that for the catalysts prereduced at lower temperatures. The sharp decrease in metal surface area (from 285 to 34 $m^2\ g^{-1}$) supports the idea that reduction of the precatalyst at 450 °C led to the burial of surface Pd into CeO_2, as previously suggested by the TPR measurements; this catalyst encapsulation is likely the result of support sintering (Figures 4 and Figure S1).

Catalysis. Hydrogenation reactions were carried out in batch mode by flowing hydrogen (~1 bar) in the headspace of a hexane solution of phenol, with a Pd to phenol mole ratio of 0.05. The results are summarized in Table 3. There was no phenol conversion when CeO_2 or PdO_xH_y/CeO_2 was used as the catalyst, confirming that Pd was crucial for hydrogen activation (entries 1 and 2). The Pd/CeO_2 catalyst hydrogenates 85.5% of the phenol with a ketone selectivity of 96.1% at room temperature and 1 bar of hydrogen in only 4 h (entry 3). These results show that Pd/CeO_2 is competitive with the best-performing catalysts reported for the liquid−solid interfacial hydrogenation of phenol.[4] Catalysts prepared in the same way using other commonly employed supports (e.g., alumina, silica, and carbon) gave significantly lower conversion under the same reaction conditions. This could be due to the weak interactions between the supports and Pd, which lead to low catalyst dispersion (Table S1 in the Supporting Information) or due to the inability to shuttle hydrogen from Pd to nonreducible supports (i.e., spillover),[51] which limits their influence on catalytic turnover. Furthermore, Pd supported on commercial ceria (surface area 55 $m^2\ g^{-1}$) was less active than Pd/CeO_2, showing the clear advantages of using a high-surface-area ceria support to promote the selective hydrogenation of phenol.

The reduction temperature used during the synthesis of Pd/CeO_2 catalyst greatly affected its activity for phenol hydrogenation. The catalysts reduced at 150, 250, and 450 °C gave significantly lower conversions than the catalyst reduced at 350 °C (Figure 5). The differences can be attributed to the dispersion and the nature of the active sites (Figure 4 and Figure S1 in the Supporting Information). The changes in TPR profiles relative to catalyst reduction temperature must reflect the changes that occur in the interactions between the metal and support. Considering that the amount of H_2 taken up during the TPR experiments significantly exceeded the stoichiometric amount required to reduce the precatalyst, the temperatures of the TPR peaks could be taken as indicators of the capacity of the catalytic sites to activate H_2. The catalysts

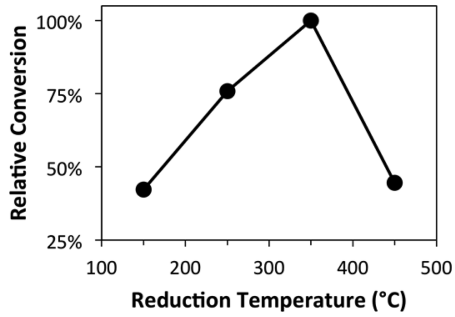

Figure 5. Relative conversion of phenol over Pd/CeO_2 as a function of PdO_xH_y/CeO_2 reduction temperature.

prepared at 250 and 350 °C gave single TPR peaks at 28 and 14 °C, and the conversion of phenol using the former as a catalyst was 76% relative to that using the latter. The catalyst reduced at 150 °C had a TPR peak at a temperature (29 °C) similar to that of the sample prepared at 250 °C; however, there was a second catalytic site, identified by a reduction peak at 95 °C, which could be responsible for lowering the conversion of phenol (42% relative to the conversion with the catalyst prepared at 350 °C). While the catalyst prepared at 450 °C had a TPR peak at 8 °C, there were also two additional peaks at 25 and 51 °C that accounted for 75% of the H_2 consumed. If the latter peaks correspond to sites that are, as suspected, buried within the CeO_2 matrix because of high-temperature reduction, then they could be responsible for the decreased conversion (44% relative to that of the catalyst prepared at 350 °C). Decreased hydrogenation efficiency upon high-temperature reduction of metal-supported ceria catalysts has also been observed for other systems and has been attributed to catalyst burial,[57,58] which could result from support sintering induced by thermal treatment under H_2.

While H_2 adsorption and activation takes place at Pd sites, phenol is expected to adsorb to the surface of the support. The high catalytic activity of Pd/CeO_2 could result not only from high dispersion of Pd and H_2 spillover onto the reducible support but also from activation of phenol upon adsorption to surface sites of CeO_2. To better understand how phenol interacts with the CeO_2 support, temperature-programmed DRIFT studies were conducted. The spectrum of CeO_2 after heating under vacuum at 150 °C showed four distinct bands at 3710, 3689, 3660, and 3554 cm^{-1} (Figure 6a). Lavalley and coworkers assigned the bands to monocoordinated OH (I) species (3710 cm^{-1}), doubly bridging OH (II) species (3657 cm^{-1}), triply bridging OH (III) species (3581 cm^{-1}), and surface-bound water (3687 cm^{-1}).[59−61] The last species was classified on the basis of the characteristic δ(OH) mode at 1631

DOI: 10.1021/cs502000j
ACS Catal. 2015, 5, 2051−2061

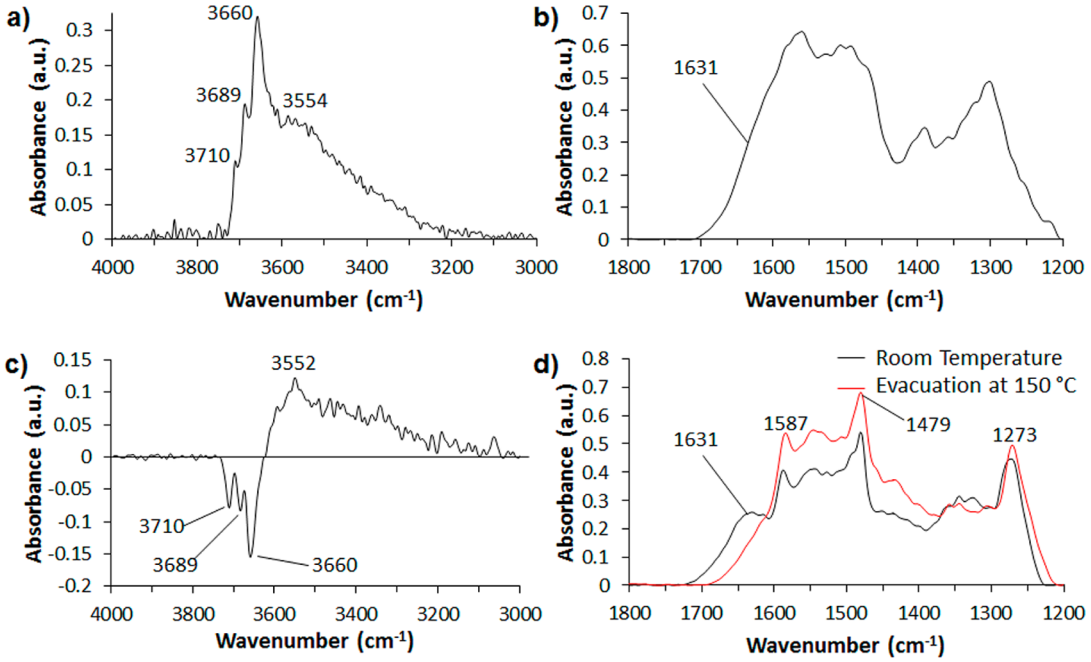

Figure 6. DRIFT spectra of CeO_2 recorded at 150 °C under evacuation from (a) 4000 to 3000 cm^{-1} and (b) 1800 to 1200 cm^{-1}. (c) DRIFT difference spectrum of CeO_2 evacuated at 150 °C and phenol adsorbed onto CeO_2 at room temperature. (d) DRIFT spectra of phenol adsorbed onto CeO_2 at room temperature and under evacuation at 150 °C.

cm^{-1} and the disappearance of the band at 3687 cm^{-1} upon evacuation at 150 °C. However, our experimental data showed no δ(OH) mode at 1631 cm^{-1} after evacuation at 150 °C (Figure 6b), while the band at 3689 cm^{-1} remained even after increasing the temperature to 200 °C. The band at 3689 cm^{-1} is likely due to the hydroxyl stretch of surface-bound hydrogen carbonate species.[62] The other peaks in Figure 6b correspond to various binding modes of carbonate from contamination during the synthesis and/or calcination in air.[62] After evacuation at 150 °C, a dilute solution of phenol in hexane was deposited onto CeO_2 at room temperature under air- and water-free conditions. The difference spectrum in the hydroxyl region clearly shows that some hydroxyl bands have disappeared, as indicated by the negative peaks at 3710, 3689, and 3660 cm^{-1} (Figure 6c). In addition, there was an emergence of a band at 1631 cm^{-1} attributed to newly formed water (Figure 6d). Evacuation at 150 °C resulted in the removal of the band at 1631 cm^{-1} (Figure 6d, red). The disappearance of hydroxyl groups and the appearance of water suggest that phenol undergoes dissociative chemisorption on ceria to form phenoxy species (Scheme 1). The formation of phenoxy species is also consistent with the basic nature of cerium dioxide.[31] The C−O stretching frequency of cerium-bound phenoxy is expected to shift relative to that of phenol,[63] and the O−H bands of phenol should not be observed. The peaks in Figure 6d at 1587, 1479, and 1273 cm^{-1} correspond to adsorbed phenyl species (Figure S3 in the Supporting Information). For comparison, the intense C−O stretching frequency of phenol occurs at 1259 cm^{-1} (Figure S4a in the Supporting Information).[64] Figure 6d shows an intense absorption band at 1273 cm^{-1}, which is attributed to the C−O stretch of a phenoxy molecule covalently bonded to a cerium cation. The increased C−O vibrational energy relative to that of phenol is consistent with the formation of cerium-bound phenoxy owing to the strong interaction expected between cationic cerium and anionic oxygen.[63] This likely results in

Scheme 1. Possible Phenol Adsorption Mechanisms on CeO_2: Dissociative Adsorption of Phenol onto Cerium Cation (a) Adjacent to a Surface Hydroxyl, (b) Containing a Surface Hydroxyl, and (c) at an Oxygen Vacancy To Produce Triply Bridging Surface Hydroxyl in Its Neighborhood

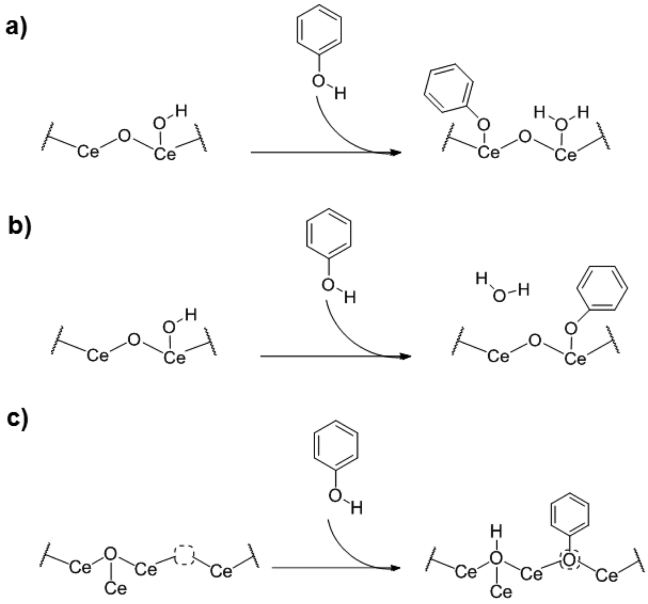

electron withdrawal from phenoxy toward the cerium cation and shortening (i.e., strengthening) of the C−O bond. The various O−H bands of phenol are typically observed at 3623, 3350, 1343, and 1207 cm^{-1}.[64] The O−H out-of-plane (1343 cm^{-1}) and intense in-plane (1207 cm^{-1}) bends are absent upon phenol adsorption onto CeO_2 (Figure S4a). In addition, Figure 6c and Figure S4b show no indication of the O−H stretch at 3623 and 3350 cm^{-1}. The only increased intensity is observed in the triply bridging hydroxyl region (3552 cm^{-1}) even after

DOI: 10.1021/cs502000j
ACS Catal. 2015, 5, 2051−2061

degassing the sample at 150 °C under vacuum (Figure S5 in the Supporting Information), which suggests new triply bridging hydroxyl groups are formed upon adsorption of phenol (Scheme 1c).[65]

The phenol adsorption analysis suggests that coordinatively unsaturated cerium cations near hydroxyl groups may be active sites for the reaction. It is not entirely clear, however, whether the newly formed water stays bound to the surface or desorbs under the reaction conditions. To address the latter, ^{1}H NMR spectroscopy studies were conducted in deuterated benzene. The CeO_2 support was degassed at 150 °C under vacuum and placed into a NMR tube containing phenol dissolved in benzene-d_6. The ^{1}H NMR spectrum showed the formation of water and decrease of phenol upon addition of CeO_2 (Figure S6 in the Supporting Information). Introduction of more CeO_2 into the same NMR tube led to an increased water signal and decreased phenol signal. Because the signals from phenol and water result from the liquid-phase species (i.e. non surface bound), it can be concluded that water desorbs from the surface of CeO_2 in benzene. However, when CeO_2 was introduced into an NMR tube containing phenol dissolved in hexane-d_{14}, phenol signals were lost from the spectra but no water was observed in the liquid phase, even though water was detected on the solid by DRIFT analysis. Thus, the water formed upon phenol adsorption on CeO_2 remains bound to the surface of the support when the reaction is performed in hexane.

The production of water upon phenol binding suggested that performing the reaction in water should affect the binding equilibrium and consequently conversion. Indeed, the catalytic activity decreased dramatically when the reaction was run in water, requiring up to 12 h to achieve 69% conversion at room temperature and 1 bar of H_2 (Table S2 in the Supporting Information). Inhibition of the reaction was likely due to adsorption of water on CeO_2 competing with phenol, thus limiting the formation of phenoxy species. Dissociative and non-dissociative adsorption of water on ceria has been shown to occur at room temperature and is even more pronounced on reduced ceria.[66] The formation and relative amounts of phenoxy species could be indirectly determined by the color change of the material, which results from the charge transfer of the bound phenoxy to cerium cations.[67] The color change of CeO_2 was obvious when it was in contact with a hexane solution of phenol but was less apparent in an aqueous solution of phenol (Figure 7a). Diffuse reflectance UV−vis measurements of the solids obtained by subtracting the contribution of CeO_2 clearly showed a higher absorbance (λ_{max} 480 nm) when hexane was used as solvent in comparison to water, an indication of higher amounts of phenoxy species present on the former (Figure 7b). These findings suggest that the increased catalytic activity in hexane relative to water may be partially due to the increased amount of phenoxy species formed on the ceria surface. The formation of a cerium-bound phenoxy group as an intermediate in the reduction can lead to a path of activation similar to that exploited by Liu,[7] Lee,[8] and Li and Luque,[11] because the direct complexation of oxygen to cerium cation results in electron withdrawal from the ring. This activation mechanism is also consistent with the increased vibrational energy of the C−O stretch of phenol adsorbed onto CeO_2 (Figure 6d).

Catalyst recycling experiments performed in hexane and water provided additional insight into the system (Figure 8). In hexane, the conversion decreased by nearly 50% after the third

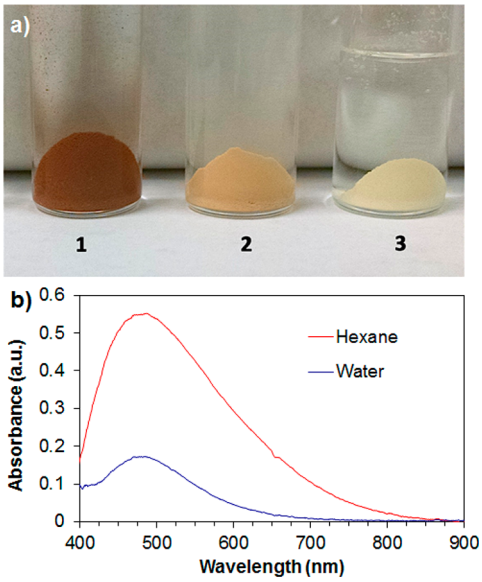

Figure 7. (a) CeO_2 samples treated with (1) a hexane solution of phenol, (2) an aqueous solution of phenol, and (3) water. (b) DR UV−vis difference spectra of CeO_2 and CeO_2 after removal from different phenol solutions.

cycle but then appeared to stabilize during subsequent reaction cycles. In water, the decrease in catalyst performance was much milder with successive cycles. After an initial decrease of about 10%, the conversion became steady in the following cycles. ICP-OES analysis of both hexane and water spent solutions had no detectable metal, indicating that leaching was not the cause of the decreased activity.[68] In addition, hot filtration experiments proved that the active phase was not homogeneous.[69,70] Interestingly, the catalytic activity could be fully recovered for both samples by regeneration via oxidation followed by reduction of the materials.

The catalysts were washed with the solvents used in the reaction, dried and analyzed by DRIFT to elucidate the types of surface species present after the conversion (Figure 9). The different possible types of surface-bound species were independently supported by DRIFT spectra of phenol, cyclohexanone, and cyclohexanol deposited onto the catalyst (Figure S3 in the Supporting Information). The bands at 3070, 1596, 1482, 1263, and 1166 cm^{-1} were assigned to adsorbed phenyl species and at 2929, 2854, 1446, 1400, and 1157 cm^{-1} to cyclohexyl species. The bands at 3699 and 3558 cm^{-1} correspond to surface hydroxyls and those at 1654, 1544, and 1236 cm^{-1} to H_2O, CO_2, and HCO_2^- on the catalyst surface, respectively (Figure S7 in the Supporting Information).[61,62] Phenyl and cyclohexyl compounds (cyclohexanone and/or cyclohexanol) were observed on the catalyst for the reaction run in hexane (black trace), while only cyclohexyl compounds were observed on the catalyst used in water (red trace). The absence of adsorbed phenyl species for the reaction in water, even if the reaction is incomplete, supports the idea that water competes for adsorption with phenyl or phenoxy species, which is consistent with the visual inspection and DR UV/vis measurements of CeO_2 treated with aqueous phenol (Figure 7). In addition, the hydroxyl band at 3699 cm^{-1} is present on the catalyst for the reaction in water but absent for the reaction in hexane. The absence of the hydroxyl band for the reaction in hexane is consistent with DRIFT analysis of phenol adsorbed onto CeO_2 (Figure 6c), and the presence of the hydroxyl band

DOI: 10.1021/cs502000j
ACS Catal. 2015, 5, 2051−2061

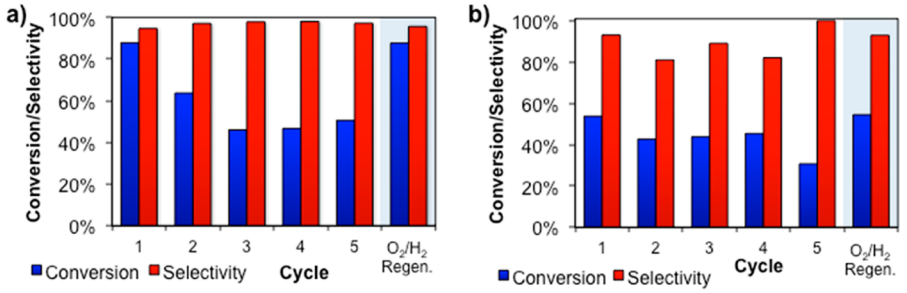

Figure 8. Cycling experiments for the hydrogenation of phenol using Pd/CeO_2 (a) in hexane at T = 25 °C and (b) in water at T = 35 °C. Reaction conditions: t = 4 h, P_{H_2} = 1 bar, Pd:phenol = 5 mol %.

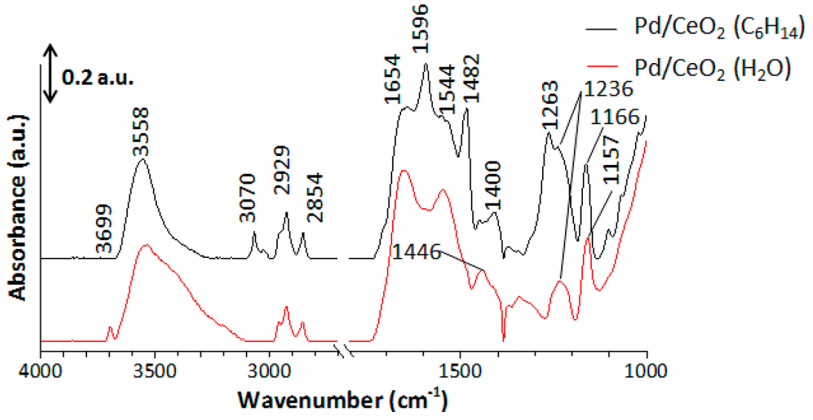

Figure 9. DRIFT spectra of Pd/CeO_2 catalysts after reaction in hexane (black) and water (red).

Scheme 2. Proposed Mechanism for Phenol Adsorption onto Ceria and Reduction by Hydrogen in Water (Left) and Hexane (Right), with Lower Structures Depicting the Binding after the First Catalytic Turnover

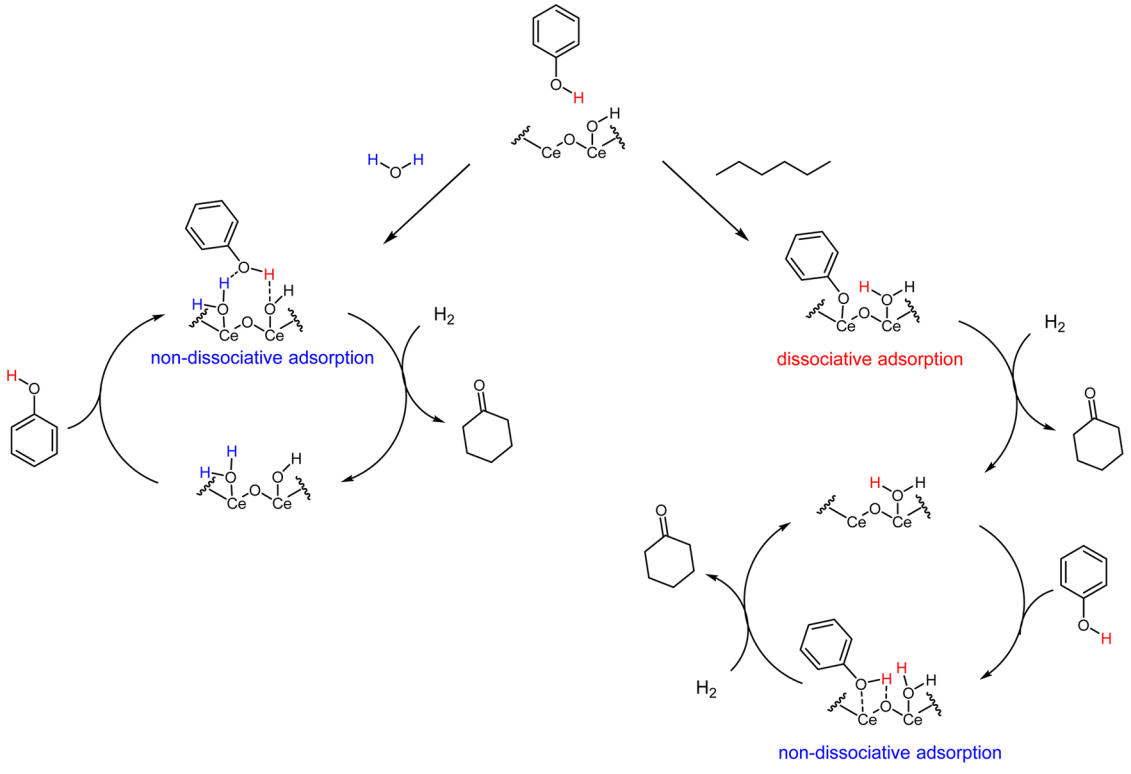

for the reaction in water is consistent with the lower amounts of phenoxy species (formed at the expense of hydroxyl species) on CeO_2 in water (Figure 7).

The transformation of ceria hydroxyl groups into water during phenol adsorption and the decreased activity upon cycling suggests that cerium cations near hydroxyls are highly

DOI: 10.1021/cs502000j
ACS Catal. 2015, 5, 2051−2061

effective sites for phenol activation in hexane and were not regenerated in situ. The data put forth suggest that the fundamental difference between catalyst activity and recyclability in water and hexane is the way in which phenol adsorbs to the CeO_2 support. While dissociative adsorption of phenol onto the support is significant in hexane, the interaction in water seems to occur mainly through physisorption, as dissociative binding is limited by competitive adsorption of water. Physisorbed phenol is expected to be less active for reduction by dissociated H_2 than phenoxy coordinated to cerium cation. The reason for this is that the cerium centers are better able to activate the phenolic ring for nucleophilic attack by dissociated H_2 because they pull more electron density away from the ring than simple hydrogen bonds with hydroxyls/water on the ceria surface. Thus, the higher activity observed in hexane should be due to the dissociative phenol adsorption and its direct binding to coordinatively unsaturated Ce cations, which is enabled by the lack of competition between substrate and solvent (Scheme 2). However, upon phenoxy formation and subsequent reduction to the ketone or alcohol, the phenoxy-forming sites were seemingly not regenerated, as indicated by the decreased activity observed in the recycling experiments. In order for the active site to be retained, a hydroxyl near a coordinatively unsaturated cerium cation should be present, which is not the case after one phenol molecule adsorbs dissociatively and is reduced (Scheme 2). The proposed deactivation mechanism is supported by the red shift of the C−O band for phenol adsorbed on the fresh (1273 cm^{-1}) and recycled (1263 cm^{-1}) catalyst (Figure S8 in the Supporting Information). In addition, the C−O band red shift on the recycled catalyst indicates that phenol is no longer able to bind dissociatively to ceria (Figure 9). The proposed solvent-dependent adsorption mechanism is consistent with the greater amounts of phenoxy species formed in hexane relative to those in water, the higher catalytic activity in hexane in comparison to that in water, the sharp decrease in activity after the first catalytic run in hexane, and the stability of catalyst activity after cycling experiments in both solvents. Furthermore, after oxidation and reduction treatment of the cycled catalyst, the DRIFT spectrum shows the reemergence of the hydroxyl peak at 3699 cm^{-1} (Figure S9 in the Supporting Information) and the activity is restored (Figure 8), further supporting the adsorption mechanism.

CONCLUSIONS

High-surface-area Pd/CeO_2 is a very active and selective catalyst for the hydrogenation of phenol to cyclohexanone at room temperature and 1 bar of hydrogen in hexane. The activity of the catalyst depends on the reduction temperature used to prepare it: the activity increases with increasing reduction temperature up to 350 °C but then decreases sharply at higher reduction temperatures. The enhanced activity at low to moderate temperatures is likely due to high dispersion of Pd as vacancies form on the surface of the support under reducing conditions. The decrease in activity at higher temperatures is likely due to support sintering that leads to catalyst encapsulation. During the catalytic reaction, phenol adsorbs dissociatively to the surface of ceria, forming cerium-bound phenoxy and water. This process likely involves hydroxyl groups in the neighborhood of the Ce sites. Conversion of the hydroxyls to water prevents dissociative adsorption in later catalytic cycles and lowers the activity of Pd/CeO_2. Nondissociative adsorption occurs when Ce sites are blocked by water and/or hydroxyls are absent in the neighborhood of the Ce sites. Chemisorbed phenoxide species are more reactive than physisorbed phenol because binding to Ce cations decreases the electron density of the aromatic ring, facilitating attack by Pd-activated hydrogen. This catalytic system constitutes a simple and efficient alternative for the production of cyclohexanone under mild reaction conditions. Since the catalyst is fully heterogeneous and does not require addition of acids or homogeneous co-catalysts, it may be a good candidate for application in continuous flow mode.

ASSOCIATED CONTENT

Supporting Information

The following file is available free of charge on the ACS Publications website at DOI: 10.1021/cs502000j.

Physical properties of all catalysts prepared, catalytic activity data for reaction in water, Pd dispersion and activity as a function of reduction temperature, additional DRIFT spectra, and NMR spectra (PDF)

AUTHOR INFORMATION

Corresponding Author

*E-mail for I.I.S.: islowing@iastate.edu.

Notes

The authors declare no competing financial interest.

ACKNOWLEDGMENTS

The authors thank BASF for the generous donation of Pluronics surfactant. This research was supported by the Critical Materials Institute, an Energy Innovation Hub funded by the U.S. Department of Energy, Office of Energy Efficiency and Renewable Energy, Advanced Manufacturing Office.

REFERENCES

(1) Fisher, W. B.; VanPeppen, J. F. In *Kirk-Othmer Encyclopedia of Chemical Technology [Online]*; Wiley: Hoboken, NJ, posted Dec 4, 2000; pp 1−7.
(2) Musser, M. T. In *Ullmann's Encyclopedia of Industrial Chemistry [Online]*; Wiley-VCH: Weinheim, Germany, posted Oct 15, 2011; pp 1−12.
(3) Rase, H. F. *Handbook of Commercial Catalysts: Heterogeneous Catalysts*; CRC Press: Boca Raton, FL, 2000; pp 128−130.
(4) Zhong, J.; Chen, J.; Chen, L. *Catal. Sci. Technol.* **2014**, *4*, 3555−3569.
(5) Buil, M. L.; Esteruelas, M. A.; Niembro, S.; Oliván, M.; Orzechowski, L.; Pelayo, C.; Vallribera, A. *Organomet.* **2010**, *29*, 4375−4383.
(6) Tang, L.-M.; Huang, M.-Y.; Jiang, Y.-Y. *Macromol. Rapid Commun.* **1994**, *15*, 527−529.
(7) Liu, H.; Jiang, T.; Han, B.; Liang, S.; Zhou, Y. *Science* **2009**, *326*, 1250−1252.
(8) Shin, J. Y.; Jung, D. J.; Lee, S.-g. *ACS Catal.* **2013**, *3*, 525−528.
(9) Cirtiu, C. M.; Dunlop-Brière, A. F.; Moores, A. *Green Chem.* **2011**, *13*, 288−291.
(10) Wang, Y.; Yao, J.; Li, H.; Su, D.; Antonietti, M. *J. Am. Chem. Soc.* **2011**, *133*, 2362−2365.
(11) Liu, H.; Li, Y.; Luque, R.; Jiang, H. *Adv. Synth. Catal.* **2011**, *353*, 3107−3113.
(12) Zhu, J.-F.; Tao, G.-H.; Liu, H.-Y.; He, L.; Sun, Q.-H.; Liu, H.-C. *Green Chem.* **2014**, *16*, 2664−2669.
(13) Chen, A.; Zhao, G.; Chen, J.; Chen, L.; Yu, Y. *RSC Adv.* **2013**, *3*, 4171−4175.
(14) Chen, J.; Zhang, W.; Chen, L.; Ma, L.; Gao, H.; Wang, T. *ChemPlusChem* **2013**, *78*, 142−148.
(15) Li, Z.; Liu, J.; Xia, C.; Li, F. *ACS Catal.* **2013**, *3*, 2440−2448.

DOI: 10.1021/cs502000j
ACS Catal. 2015, 5, 2051−2061

(16) Cheng, L.; Dai, Q.; Li, H.; Wang, X. *Catal. Commun.* **2014**, *57*, 23−28.
(17) Deshmukh, R. R.; Lee, J. W.; Shin, U. S.; Lee, J. Y.; Song, C. E. *Angew. Chem., Int. Ed.* **2008**, *47*, 8615−8617.
(18) Panagiotopoulou, P.; Kondarides, D. I. *Catal. Today* **2006**, *112*, 49−52.
(19) *Catalysis by Ceria and Related Materials*; Trovarelli, A., Ed.; Imperial College Press: London, 2002; Vol. *2*.
(20) Trovarelli, A. *Catal. Rev.* **1996**, *38*, 439−520.
(21) Trovarelli, A.; de Leitenburg, C.; Boaro, M.; Dolcetti, G. *Catal. Today* **1999**, *50*, 353−367.
(22) Aneggi, E.; Wiater, D.; de Leitenburg, C.; Llorca, J.; Trovarelli, A. *ACS Catal.* **2014**, *4*, 172−181.
(23) Li, W. B.; Wang, J. X.; Gong, H. *Catal. Today* **2009**, *148*, 81−87.
(24) Fan, L.; Wang, C.; Chen, M.; Zhu, B. *J. Power Sources* **2013**, *234*, 154−174.
(25) Ratnasamy, C.; Wagner, J. P. *Catal. Rev.* **2009**, *51*, 325−440.
(26) Si, R.; Flytzani-Stephanopoulos, M. *Angew. Chem., Int. Ed.* **2008**, *47*, 2884−2887.
(27) Gamarra, D.; Belver, C.; Fernández-García, M.; Martínez-Arias, A. *J. Am. Chem. Soc.* **2007**, *129*, 12064−12065.
(28) Murugan, B.; Ramaswamy, A. V. *J. Am. Chem. Soc.* **2007**, *129*, 3062−3063.
(29) Beckers, J.; Rothenberg, G. *Green Chem.* **2010**, *12*, 939−948.
(30) Vivier, L.; Duprez, D. *ChemSusChem* **2010**, *3*, 654−678.
(31) Andreeva, D.; Tabakova, T.; Ilieva, L. In *Catalysis by ceria and related materials*, 2nd ed.; Trovarelli, A., Fornasiero, P., Eds.; Imperial College Press: London, 2013; Vol. *12*, pp 497−564.
(32) Velu, S.; Kapoor, M. P.; Inagaki, S.; Suzuki, K. *Appl. Catal., A* **2003**, *245*, 317−331.
(33) Scirè, S.; Minicò, S.; Crisafulli, C. *Appl. Catal., A* **2002**, *235*, 21−31.
(34) Li, H.; Liu, J.; Xie, S.; Qiao, M.; Dai, W.; Lu, Y.; Li, H. *Adv. Funct. Mater.* **2008**, *18*, 3235−3241.
(35) Liu, J.; Li, H.; Li, H. *Chin. J. Catal.* **2007**, *28*, 312−316.
(36) Davis, M. E. *Nature* **2002**, *417*, 813−821.
(37) Kandel, K.; Frederickson, C.; Smith, E. A.; Lee, Y.-J.; Slowing, I. I. *ACS Catal.* **2013**, *3*, 2750−2758.
(38) Yuan, Q.; Yin, A.-X.; Luo, C.; Sun, L.-D.; Zhang, Y.-W.; Duan, W.-T.; Liu, H.-C.; Yan, C.-H. *J. Am. Chem. Soc.* **2008**, *130*, 3465−3472.
(39) Shyu, J. Z.; Otto, K.; Watkins, W. L. H.; Graham, G. W.; Belitz, R. K.; Gandhi, H. S. *J. Catal.* **1988**, *114*, 23−33.
(40) Brinker, C. J.; Lu, Y.; Sellinger, A.; Fan, H. *Adv. Mater.* **1999**, *11*, 579−585.
(41) Fan, J.; Boettcher, S. W.; Stucky, G. D. *Chem. Mater.* **2006**, *18*, 6391−6396.
(42) Meng, Y.; Gu, D.; Zhang, F.; Shi, Y.; Cheng, L.; Feng, D.; Wu, Z.; Chen, Z.; Wan, Y.; Stein, A.; Zhao, D. *Chem. Mater.* **2006**, *18*, 4447−4464.
(43) Grosso, D.; Cagnol, F.; Soler-Illia, G. J. d. A. A.; Crepaldi, E. L.; Amenitsch, H.; Brunet-Bruneau, A.; Bourgeois, A.; Sanchez, C. *Adv. Funct. Mater.* **2004**, *14*, 309−322.
(44) Perrichon, V.; Laachir, A.; Abouarnadasse, S.; Touret, O.; Blanchard, G. *Appl. Catal., A* **1995**, *129*, 69−82.
(45) Peterson, E. J.; DeLaRiva, A. T.; Lin, S.; Johnson, R. S.; Guo, H.; Miller, J. T.; Hun Kwak, J.; Peden, C. H. F.; Kiefer, B.; Allard, L. F.; Ribeiro, F. H.; Datye, A. K. *Nat. Commun.* **2014**, *5*, 4885.
(46) Gulyaev, R. V.; Slavinskaya, E. M.; Novopashin, S. A.; Smovzh, D. V.; Zaikovskii, A. V.; Osadchii, D. Y.; Bulavchenko, O. A.; Korenev, S. V.; Boronin, A. I. *Appl. Catal., B* **2014**, *147*, 132−143.
(47) Bernal, S.; Calvino, J. J.; Cauqui, M. A.; Gatica, J. M.; Larese, C.; Pérez Omil, J. A.; Pintado, J. M. *Catal. Today* **1999**, *50*, 175−206.
(48) Giordano, F.; Trovarelli, A.; de Leitenburg, C.; Giona, M. *J. Catal.* **2000**, *193*, 273−282.
(49) Luo, M.-F.; Hou, Z.-Y.; Yuan, X.-X.; Zheng, X.-M. *Catal. Lett.* **1998**, *50*, 205−209.
(50) Bensalem, A.; Bozon-Verduraz, F.; Perrichon, V. *J. Chem. Soc., Faraday Trans.* **1995**, *91*, 2185−2189.
(51) Prins, R. *Chem. Rev.* **2012**, *112*, 2714−2738.
(52) Sanchez, M. G.; Gazquez, J. L. *J. Catal.* **1987**, *104*, 120−135.
(53) Kepinski, L.; Wolcyrz, M.; Okal, J. *J. Chem. Soc., Faraday Trans.* **1995**, *91*, 507−515.
(54) Bernal, S.; Botana, F. J.; Calvino, J. J.; Cauqui, M. A.; Cifredo, G. A.; Jobacho, A.; Pintado, J. M.; Rodriguez-Izquierdo, J. M. *J. Phys. Chem.* **1993**, *97*, 4118−4123.
(55) Ta, N.; Liu, J.; Chenna, S.; Crozier, P. A.; Li, Y.; Chen, A.; Shen, W. *J. Am. Chem. Soc.* **2012**, *134*, 20585−20588.
(56) Farmer, J. A.; Campbell, C. T. *Science* **2010**, *329*, 933−936.
(57) Cunningham, J.; O'Brien, S.; Sanz, J.; Rojo, J. M.; Soria, J. A.; Fierro, J. L. G. *J. Mol. Catal.* **1990**, *57*, 379−396.
(58) Barrault, J.; Alouche, A.; Paul-Boncour, V.; Hilaire, L.; Percheron-Guegan, A. *Appl. Catal.* **1989**, *46*, 269−279.
(59) Laachir, A.; Perrichon, V.; Badri, A.; Lamotte, J.; Catherine, E.; Lavalley, J. C.; El Fallah, J.; Hilaire, L.; Le Normand, F.; Quemere, E.; Sauvion, G. N.; Touret, O. *J. Chem. Soc., Faraday Trans.* **1991**, *87*, 1601−1609.
(60) Badri, A.; Binet, C.; Lavalley, J.-C. *J. Chem. Soc., Faraday Trans.* **1996**, *92*, 4669−4673.
(61) Binet, C.; Daturi, M.; Lavalley, J.-C. *Catal. Today* **1999**, *50*, 207−225.
(62) Vayssilov, G. N.; Mihaylov, M.; Petkov, P. S.; Hadjiivanov, K. I.; Neyman, K. M. *J. Phys. Chem. C* **2011**, *115*, 23435−23454.
(63) Wu, Z.; Li, M.; Mullins, D. R.; Overbury, S. H. *ACS Catal.* **2012**, *2*, 2224−2234.
(64) Nguyen, M. T.; Kryachko, E. S.; Vanquickenborne, L. G. In *The Chemistry of Phenols Part 1*; Rappoport, Z., Ed.; Wiley: West Sussex, England, 2003; pp 31−48.
(65) Hansen, H. A.; Wolverton, C. *J. Phys. Chem. C* **2014**, *118*, 27402−27414.
(66) Mullins, D. R.; Albrecht, P. M.; Chen, T.-L.; Calaza, F. C.; Biegalski, M. D.; Christen, H. M.; Overbury, S. H. *J. Phys. Chem. C* **2012**, *116*, 19419−19428.
(67) Sharpe, E.; Frasco, T.; Andreescu, D.; Andreescu, S. *Analyst* **2013**, *138*, 249−262.
(68) Phan, N. T. S.; Van Der Sluys, M.; Jones, C. W. *Adv. Synth. Catal.* **2006**, *348*, 609−679.
(69) Richardson, J. M.; Jones, C. W. *J. Catal.* **2007**, *251*, 80−93.
(70) Ji, Y.; Jain, S.; Davis, R. J. *J. Phys. Chem. B* **2005**, *109*, 17232−17238.

DOI: 10.1021/cs502000j
ACS Catal. 2015, 5, 2051−2061